Accurate modeling of the dynamics of dissociative chemisorption on metal surfaces

Gerrits, N.

Chapter 9

Dissociative Chemisorption of CHD_3 on Pd(111)

This chapter is based on Gerrits, N.; Chadwick, H.; Kroes, G.-J. Dynamical Study of the Dissociative Chemisorption of CHD_3 on Pd(111). *J. Phys. Chem. C* **2019**, *123*, 24013–24023, DOI: 10.1021/acs.jpcc.9b05757

Abstract

The specific reaction parameter (SRP) approach to density functional theory has been shown to model reactions of polyatomic molecules with metal surfaces important for heterogeneous catalysis in industry with chemical accuracy. However, transferability of the SRP functional among systems in which methane interacts with group 10 metals remains unclear for methane + Pd(111). Therefore, in this chapter, predictions have been made for the reaction of CHD_3 on Pd(111) using Born-Oppenheimer molecular dynamics, while also performing a rough comparison with experimental data for CH_4 + Pd(111) obtained for lower incidence energies. Hopefully, future experiments can test the transferability of the SRP functional among group 10 metals also for Pd(111). It has been found that the reactivity of CHD_3 on Pd(111) is intermediate between and similar to either Pt(111) or Ni(111), depending on the incidence energy and the initial vibrational state distribution. This is surprising because the barrier height and experiments performed at lower incidence energies than investigated here suggest that the reactivity of Pd(111) should be similar to that of Pt(111) only. The relative decrease in the reactivity of Pd(111) at high incidence energies can be understood from the site specificity of the reaction and from dynamical effects such as the bobsled effect and energy transfer from methane to the surface.

9.1 Introduction

An important heterogeneously catalyzed industrial process is steam reforming, where methane and steam react over a metal catalyst (typically Ni[1]) and subsequently form carbon monoxide and hydrogen. At high temperature, the dissociation of methane, i.e., breaking the first CH bond, is a rate-controlling state in steam reforming on a wide variety of metals[2, 3]. Therefore, a detailed study of the CH bond breaking is warranted in order to improve catalysts. However, the reaction of molecules on metal surfaces remains difficult to simulate due to the complexity of molecule-metal surface interactions[4–8]. The so-called specific reaction parameter (SRP) approach to density functional theory (DFT), though, has been shown to provide chemically accurate results, i.e., with errors smaller than 1 kcal/mol (4.2 kJ/mol), for a number of molecule-metal surface reactions[9–14].

Within the SRP-DFT approach, two density functionals are mixed, of which one overestimates and one underestimates the reaction probability, according to an empirically determined parameter in order to create an SRP functional. Recently, an SRP functional was developed (the SRP32-vdW functional) that gave chemically accurate results not only for the molecule-metal surface reaction it was developed for (CHD_3 + Ni(111)[12]), but also for methane interacting with a metal from the same periodic table group (CHD_3 + Pt(111)[13]) and with a stepped surface of Pt (CHD_3 + Pt(211)[13–15]). However, it remains unclear whether this transferability is common among all group 10 metals. Therefore, in this chapter, predictive Born-Oppenheimer molecular dynamics (BOMD) calculations have been performed for CHD_3 + Pd(111) with the SRP32-vdW functional in the hope that future experiments will test the transferability of the SRP functional describing methane interacting with all group 10 metal surfaces. Although in previous work direct dynamics calculations with SRP functionals is usually referred to as "ab initio molecular dynamics" (AIMD) calculations, the wording of the method is changed here from AIMD to BOMD as "ab initio" can be misleading in the context of calculations based on a semi-empirical density functional.

To ensure the validity of the BOMD method, conditions are adressed for which the total energy of the molecule (translational + vibrational) exceeds the minimum zero-point energy corrected barrier height of the system addressed. This ensures that the accuracy of the quasi-classical trajectory (QCT) method used in the BOMD dynamics is not much affected by quantum effects like tunneling, and classical artifacts like zero-point energy violation[16, 17]. Second, for laser-off conditions, only conditions are adressed where at least 60% of the incident CHD_3 is in its initial vibrational ground state, and in predictions

for initial-state selective reaction only CH stretch excited CHD_3 is adressed, to avoid problems with artificial intramolecular vibrational redistribution (IVR) that might otherwise affect QCT calculations[18, 19]. Third, the surface temperature employed (here, 500 K) is well above the surface Debye temperature ((140 ± 10) K for Pd(111))[20], thereby ensuring that the energy transfer between the molecule and surface can be well described with quasi-classical dynamics[13, 21, 22].

Also, a rough comparison is performed with existing experimental data for CH_4 + Pd(111)[23], although a direct comparison is not possible due to the low experimental reaction probabilities making BOMD calculations untractable and the employed high nozzle temperatures for which BOMD performs badly due to IVR among excited vibrational states[12].

Alloys are of special interest for catalysts[24] as they can increase both reactivity and selectivity[25]. For example, by combining a highly active metal like Pt with a less reactive metal such as Cu, a catalyst with a high activity and selectivity can be produced, without the typical issues such as catalyst poisoning[26]. The work in Chapter 7 has predicted that the Pt-Cu(111) single-atom alloy is considerably more reactive than Pd-Cu(111), even though the barrier height difference is only 8.4 kJ/mol. It was suggested that dynamical effects such as the "bobsled effect"[27, 28] played a major role in the relatively lower reactivity of Pd-Cu(111) compared to that of Pt-Cu(111)[29]. The so-called bobsled effect causes molecules with a high incidence energy to slide off the minimum energy path (MEP) for late barrier systems as the molecule is not able to make the turn in front of the barrier on the potential energy surface (PES) and therefore needs to overcome a higher barrier than the lowest barrier available[27, 28]. Since it was shown that the barrier geometries and potential energy surfaces (PES) above the doped atoms were similar to those found for the pure (111) surfaces of the respective doped elements, these dynamical effects can also be investigated by comparing methane interacting with Pd(111) and Pt(111).

The reaction of methane on metal surfaces remains fundamentally important due to many dynamically interesting effects. For example, in partially deuterated methane, the CH bond can selectively be broken by exciting the CH stretch mode[12, 13, 30–33]. Also, the dissociative chemisorption of methane is vibrational-mode-specific[34, 35] and the mode specificity is dependent on the metal surface[35–37]. Moreover, steric effects play a significant role[38]. Finally, the reaction of methane is site specific[2, 13, 15, 39]. For all of these reasons, in this chapter a detailed analysis is presented of the results from the BOMD calculations on the dissociative chemisorption of CHD_3 on Pd(111), and a comparison is made to the results obtained on Pt(111) and Ni(111).

9.2 Method

For the BOMD and electronic structure (DFT) calculations, the Vienna Ab-initio Simulation Package (VASP version 5.3.5)[40–44] is used. The first Brillouin zone is sampled by a Γ-centered $6 \times 6 \times 1$ k-point grid and the plane wave basis set kinetic energy cutoff is 400 eV. Moreover, the core electrons have been represented with the projector augmented wave (PAW) method[44, 45]. The surface is modeled using a 4 layer (3×3) supercell, where the top three layers have been relaxed in the Z direction and a vacuum distance of 13 Å is used between the slabs. Due to the computational cost, a small vacuum distance (i.e., 13 Å) is required, which effectively raises the barrier height by 4.9 kJ/mol. Therefore, 4.9 kJ/mol is added to the translational energy to counteract this shift (see Section 2.4.2). To speed up convergence, first-order Methfessel-Paxton smearing[46] with a width parameter of 0.2 eV has been applied. The employed computational setup is confirmed to be converged within chemical accuracy (4.2 kJ/mol), as shown by the convergence tests provided in Section 9.A.

The transition state (TS) is obtained with the dimer method[47–50] as implemented in the VASP Transition State Tools package (VTST)[51], and is confirmed to be a first-order saddle point. Forces are converged within 5 meV/Å, where only the methane is relaxed.

The SRP32-vdW functional is employed, which has been previously used for CHD_3 + Ni(111), Pt(111), Pt(211), Pt(110), Pt(210), Cu(111) and Cu(211) as well[12–14, 29, 52–55]. The exchange functional is defined as

$$E_x = x \cdot E_x^{RPBE} + (1 - x) \cdot E_x^{PBE}, \tag{9.1}$$

where E_x^{PBE} and E_x^{RPBE} are the exchange parts of the Perdew, Burke and Ernzerhof (PBE)[56] and revised PBE (RPBE)[57] exchange-correlation functionals, respectively, and $x = 0.32$. Since it has been shown that modeling Van der Waals interactions is vital for describing the reaction of methane on a metal surface[13, 14], the vdW correlation functional of Dion and coworkers (vdW-DF1)[58] is used.

A surface temperature of 500 K is simulated in the BOMD calculations, where the atoms in the top three layers are allowed to move and the expansion of the bulk due to the surface temperature is simulated by expanding the computed ideal lattice constant[59] (3.99 Å) by a factor of 1.0049[60]. The parameters used to simulate the molecular beams are taken from Ref. [13] (see Table 9.1), which describes experiments performed for CHD_3 + Pt(111), except for Ni(111) at $\langle E_i \rangle = 101.1$ kJ/mol, for which the parameters are taken

TABLE 9.1: Experimental beam parameters that describe the simulated CHD_3 velocity distributions for Pt(111). ν_0 and α are determined through time-of-flight measurements[13]. For $T_n = 550\,K$ the parameters are taken from Ref. [12] for Ni(111).

T_n (K)	$\langle E_i \rangle$ kJ/mol	ν_0 (m/s)	α (m/s)
350	71.4	2723	149
450	89.2	3026	246
500	97.4	3157	270
550	101.0	3240	174
550	102.5	3231	299
600	111.9	3369	333
650	120.0	3483	367

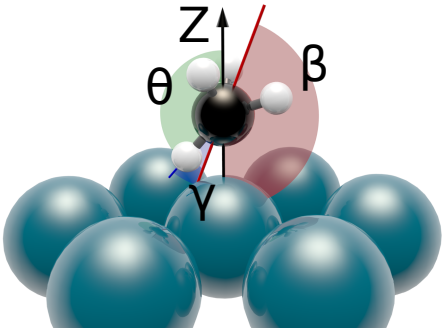

FIGURE 9.1: TS of methane on Pd(111), indicating the orientation angles as used in Table 9.2. θ is the angle between the CH-bond and the surface normal, β is the angle between the umbrella axis and the surface normal, and γ is the angle between θ and β (see text for further explanation).

from Ref. [12] (experiments performed for CHD_3 + Ni(111)). For every BOMD data point, between 500 and 1000 trajectories were run, with a time step of 0.4 fs, for a maximum total time of 1 ps. Other technical details of the BOMD calculations and the sampling of the initial conditions can be found in recent work[12, 13, 16] and in Chapter 2.

9.3 Results

9.3.1 Activation Barriers

The barrier heights and geometries of CHD_3 on Pd(111) are compared to the barrier data on Ni(111) and Pt(111) in Table 9.2. θ is the angle between the

TABLE 9.2: Minimum barrier geometries and heights of methane on Ni(111)[12], Pd(111) and Pt(111)[13]. The zero-point energy corrected barrier heights are given in brackets.

Surface	Site	Z_C (Å)	r (Å)	θ (°)	β (°)	γ (°)	E_b (kJ/mol)
Ni(111)	Top[12]	2.18	1.61	135.7	164.7	29.1	97.9 (85.3)
Ni(111)	Fcc	2.09	1.63	128.5	157.3	30.7	121.1 (105.5)
Ni(111)	Hcp	2.16	1.74	132.9	167.8	35.6	134.6 (120.7)
Ni(111)	Bridge	2.06	1.65	126.3	154.8	29.5	135.1 (120.5)
Ni(111)	T2f	2.07	1.90	126.5	171.1	45.3	99.1 (88.8)
Ni(111)	T2b	2.12	1.63	130.4	160.0	31.0	113.9 (99.1)
Pd(111)	Top	2.23	1.61	135.9	165.0	29.1	84.1 (70.1)
Pd(111)	Fcc	2.14	1.73	133.0	160.8	27.8	132.6 (116.9)
Pd(111)	Hcp	2.18	1.75	133.8	161.5	27.7	133.6 (118.1)
Pd(111)	Bridge	2.14	1.76	130.8	161.9	31.1	125.6 (110.9)
Pd(111)	T2f	2.17	1.82	137.5	178.0	40.6	108.4 (96.1)
Pd(111)	T2b	2.18	1.76	132.8	165.8	33.0	132.5 (118.3)
Pt(111)	Top[13]	2.28	1.56	133	168	35	78.7 (66.5)
Pt(111)	Fcc	2.47	1.91	139.7	166.9	27.2	163.5 (145.8)
Pt(111)	Hcp	2.59	1.90	122.1	161.2	39.1	158.0 (144.7)
Pt(111)	Bridge	2.36	1.77	136.2	164.3	29.0	146.2 (128.1)
Pt(111)	T2f	2.31	1.64	149.5	179.2	29.7	117.7 (101.6)
Pt(111)	T2b	2.45	1.81	140.5	172.6	32.0	152.9 (136.5)

dissociating bond and the surface normal, β is the angle between the surface normal and the umbrella axis, which is defined as the vector going from the geometric center of the three non-dissociating hydrogen atoms to the carbon atom, and γ indicates the angle between the umbrella axis and the dissociating bond (see Figure 9.1). The minimum barrier geometry on Pd(111) is similar to the minimum barrier geometry on Ni(111), with the main difference being that the barrier on Pd is at a larger distance from the surface than on Ni. However, the barrier height on Pd is much closer to that on Pt(111), being only 5.4 kJ/mol higher than on Pt(111). Based on the minimum barrier heights reported in Table 9.2, it is to be expected that the reactivity of Pd(111) is closest to that of Pt(111). Furthermore, the lowest barrier is located on the top site, which is typical for methane on a metal surface[12, 13, 29, 61].

Moreover, barriers are also obtained above the fcc, hcp, bridge, top-2-fcc (t2f), and top-2-bridge (t2b) sites, by fixing the carbon atom in the X and Y directions above the aforementioned sites. Here, the t2f and t2b sites are midway between the hcp and fcc, and hcp and bridge sites, respectively. For these barrier geometries, the angles are similar, but the length of the dissociating bond does increase, making the barrier even later. The distance of the carbon atom to the surface is smaller for Pd(111) and Ni(111) than at the top site, whereas in most cases it is larger for Pt(111). For Pt(111), the obtained barrier heights at the sites other than the top site are considerably higher than those of Pd(111) and Ni(111). The general trend observed here is that when going from Ni(111) to Pt(111), the difference between the barrier heights at the top site and at the other sites increases. Furthermore, among the sites other than the top sites, the lowest barrier occurs on the t2f site for all metals. For Ni(111), this barrier is almost as low as the top site so that it may play an important role in the dynamics.

Finally, the adsorption energies of CH_3 and H on Pd(111) are compared to those on Ni(111) and Pt(111) in Tables 9.3 and 9.4. For CH_3, Pd(111) is an intermediate of Ni(111) and Pt(111). The difference between the adsorption energies at the hollow and top sites is smaller for Pd(111) than for Pt(111), but for both the preferred site is the top site, as opposed to Ni(111) where the preferred sites are the hollow sites. This may also explain why the barrier for dissociation on the t2f site is so low on Ni(111). However, Pd(111) is very similar to Ni(111) concerning the adsorption of hydrogen, where the binding of hydrogen to the top site is considerably weaker than to the other sites.

TABLE 9.3: Adsorption energy of CH_3 on Ni(111)[62], Pd(111) and Pt(111)[62]. Note that the adsorption energies on Ni(111) and Pt(111) were calculated with the PBE functional.

Surface	Site	Z_C (Å)	Adsorption energy (kJ/mol)
Ni(111)[62]	Bridge	1.69	-155.2
Ni(111)[62]	Fcc	1.55	-175.2
Ni(111)[62]	Hcp	1.56	-172.5
Ni(111)[62]	Top	1.98	-143.9
Pd(111)	Bridge	1.85	-158.2
Pd(111)	Fcc	1.75	-160.5
Pd(111)	Hcp	1.77	-152.9
Pd(111)	Top	2.09	-188.4
Pt(111)[62]	Bridge	1.86	-120.2
Pt(111)[62]	Fcc	1.78	-115.2
Pt(111)[62]	Hcp	1.82	-105.4
Pt(111)[62]	Top	2.10	-180.8

TABLE 9.4: Adsorption energy of H on Ni(111)[62], Pd(111) and Pt(111)[62]. Note that the adsorption energies on Ni(111) and Pt(111) were calculated with the PBE functional.

Surface	Site	Z_H (Å)	Adsorption energy (kJ/mol)
Ni(111)[62]	Bridge	1.04	-256.4
Ni(111)[62]	Fcc	0.91	-270.2
Ni(111)[62]	Hcp	0.91	-269.3
Ni(111)[62]	Top	1.47	-212.8
Pd(111)	Bridge	0.98	-255.2
Pd(111)	Fcc	0.81	-268.0
Pd(111)	Hcp	0.81	-262.7
Pd(111)	Top	1.56	-223.9
Pt(111)[62]	Bridge	1.06	-256.5
Pt(111)[62]	Fcc	0.92	-261.3
Pt(111)[62]	Hcp	0.91	-256.5
Pt(111)[62]	Top	1.56	-257.2

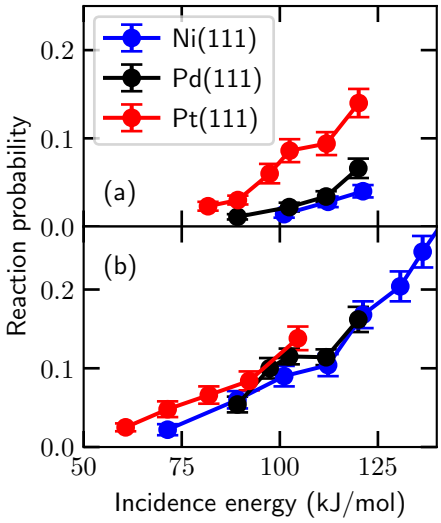

FIGURE 9.2: Reaction probability of CHD_3 on Ni(111) (blue), Pd(111) (black) and Pt(111) (red) for laser-off (a) and $\nu_1 = 1$ (b) using BOMD simulations. Results for Ni(111) and Pt(111) are taken from Refs. [12] and [13], respectively. The error bars represent 68% confidence intervals.

9.3.2 Sticking Probability

Results for the reaction of methane on Pd(111) using BOMD are compared to those on Ni(111) and Pt(111) in Figure 9.2 for laser-off conditions and $\nu_1 = 1$ (exciting the CH stretch mode with one quantum). Note that three additional points for Ni(111) have been calculated at $\langle E_i \rangle = 71.4$, 89.2, and 101.1 kJ/mol for $\nu_1 = 1$ using the same computational set up as in Ref. [12]. Additionally, results for $\langle E_i \rangle = 146.6$ kJ/mol were obtained in the original work of Ref. [12], but have not been reported before because there were no experimental data for this incidence energy. Contrary to expectations based on the minimum barrier heights only (see Table 9.2), for laser-off conditions the reaction probability on Pd(111) is similar to that on Ni(111). It should be noted that for Ni(111) a slightly higher surface temperature is used (550 K) than for Pd(111) and Pt(111) (500 K). However, this should not affect the results considerably as the surface temperature does not play a large role at high incidence energies, which will be discussed more in-depth in Section 9.3.4. For $\nu_1 = 1$ at lower incidence energy, the reaction probability is similar on all three systems investigated. Interestingly, on Pd(111) the reaction probability does not increase from 102 to 112 kJ/mol. It is possible that this is related to the site-dependence of the reaction, which will be discussed later in Section 9.3.3. The generally much lower laser-off reactivity of Pd(111) compared to that of Pt(111) at high incidence energy is also consistent with the prediction that Pt-Cu(111) is much more reactive than Pd-Cu(111) at high incidence energies[29].

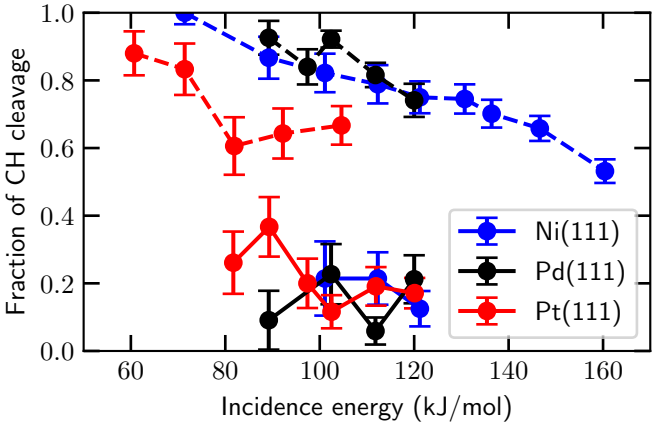

FIGURE 9.3: Fraction of reactions that occurred through CH bond cleavage for CHD_3 on Ni(111) (blue), Pd(111) (black), and Pt(111) (red). Laser-off and $\nu_1 = 1$ results are indicated by solid and dashed lines, respectively. The error bars represent 68% confidence intervals.

Finally, we note that the trapping probabilities are not included in the reaction probability, as they are smaller than 0.5%.

The bond selectivity is shown in Figure 9.3, where the fraction of CH bond cleavage under laser-off and state-resolved $\nu_1 = 1$ conditions are compared. When the CH stretch mode is excited the dissociation of CHD_3 is very selective towards CH cleavage, whereas under laser-off conditions CH cleavage is close to statistical (25%). This is similar to what has been observed for CHD_3 + Ni(111)[12, 30] and CHD_3 + Pt(111)[13]. However, it remains unclear why on Pd(111) for laser-off conditions the fraction of CH cleavage is considerably lower for 112 kJ/mol compared to the other incidence energies under laser-off conditions. This may well be a statistical anomaly since a statistical analysis using Fisher's exact test[63] cannot reject the null hypothesis that the CH dissociation probability is the same for all incidence energies. Moreover, at higher incidence energies and laser-off conditions, the CH cleavage ratio is somewhat lower than 0.25, which is attributed to the presence of CD-excited vibrational states in the beam[12] (note that there may be some artificial energy flow between these modes in classical dynamics calculations).

Finally, the obtained vibrational efficacies of CHD_3 on Ni(111), Pd(111) and Pt(111) are shown in Table 9.5. Generally, Ni(111) yields the highest vibrational efficacy, whereas Pt(111) yields the lowest vibrational efficacy.

TABLE 9.5: Vibrational efficacy ($\nu_1 = 1$) of CHD_3 on Ni(111), Pd(111) and Pt(111) as a function of the reaction probability.

Surface	Reaction probability (%)	Vibrational efficacy
Ni(111)	2.8	0.9 - 1.3
Ni(111)	4.0	0.9 - 1.3
Pd(111)	5.4	0.7 - 0.9
Pd(111)	6.6	0.7 - 0.9
Pt(111)	3.6	0.8
Pt(111)	4.7	0.6
Pt(111)	5.4	0.6
Pt(111)	7.1	0.5
Pt(111)	10.0	0.3

TABLE 9.6: Average value of the θ, β and γ angles with the standard error (σ_m) and standard deviation (σ) for all laser-off and $\nu_1 = 1$ reacted trajectories when a dissociating bond reaches the TS value.

Surface	$\theta(^\circ) \pm \sigma_m(\sigma)$	$\beta(^\circ) \pm \sigma_m(\sigma)$	$\gamma(^\circ) \pm \sigma_m(\sigma)$
Ni(111)	117.0 ± 0.3 (11.3)	142.1 ± 0.4 (13.6)	31.3 ± 0.3 (12.4)
Pd(111)	123.5 ± 0.5 (11.0)	143.9 ± 0.6 (14.1)	27.9 ± 0.5 (11.4)
Pt(111)	123.5 ± 0.5 (10.1)	150.0 ± 0.6 (12.2)	34.1 ± 0.6 (12.8)

9.3.3 Dynamics of the Reaction

Distribution of the angles indicated in Figure 9.1 are shown in Figure 9.4 and average values are shown in Table 9.6 for the reacted trajectories. It is observed that both the initial θ and β angles, i.e., the angles that describe the orientations of the dissociating bond and umbrella axis, are close to the TS geometry. Moreover, during the dynamics, a considerable amount of bending between the dissociating bond and umbrella axis (γ angle) is observed. Finally, for all the angles considered some steering is observed, in the sense that at the time of reaction the distributions describing the reacting molecules have moved somewhat towards the TS value of the angle described. However, the reaction is not rotationally adiabatic (at the initial time step the orientation distribution of the reacting molecule is not statistical), in agreement with previous observations for Ni(111)[12] and Pt(111)[13]. This has consequences for how the rotations should be treated[5] in the reaction path Hamiltonian (RPH)

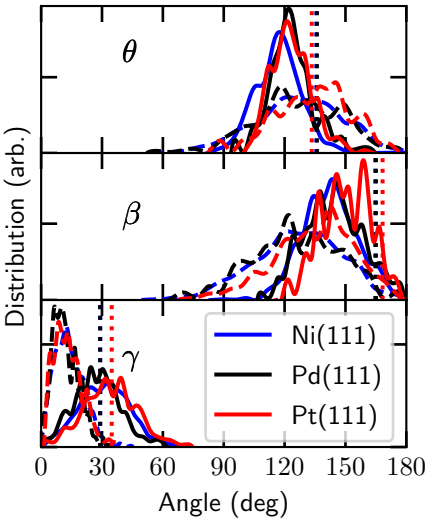

FIGURE 9.4: Distributions of the θ, β and γ angles of methane during BOMD for all laser-off and $\nu_1 = 1$ reacted trajectories at the initial time step (dashed line) and when a dissociating bond reaches the TS value (solid line). The dotted lines indicate the TS values (note that Ni(111) and Pd(111) yield almost identical values). Blue is Ni(111)[12], black is Pd(111), and red is Pt(111)[13]

approach of Jackson and coworkers[64]. Furthermore, the aforementioned dynamical behaviour of the angles is not only typical for methane reacting on a group 10 metal surface (as can be seen in Figure 9.4), but also for methane reacting on Cu(111)[29] (see Chapter 7).

Although the barrier height on Pd(111) is considerably lower than on Ni(111), the barrier geometries are similar and thus dynamical effects such as the bobsled effect[27, 28] would be expected to play similar roles. That the bobsled effect plays a role in the reaction of CHD_3 on group 10 metal surfaces can be seen in Figure 9.5, where the distance of the carbon atom to the surface is shown at the time of dissociation. Both laser-off and $\nu_1 = 1$ trajectories that go on to react tend to slide off the MEP due to the bobsled effect and thus react over higher barriers. This deviation from the MEP increases with incidence energy, which is observed above all high-symmetry sites and thus is not related to the site over which the methane reacts. Furthermore, the bobsled effect is considerably smaller for Pt(111) than for Pd(111) and Ni(111), which leads to methane having to react over relatively higher barriers on Pd(111) and Ni(111) than on Pt(111) (see Figure 9.5).

For similar values of the reaction probability, the bobsled effect on the reaction dynamics of CHD_3 under laser-off conditions (predominantly $\nu_1 = 0$) is larger than for $\nu_1 = 1$. The reason is that a larger incidence energy is required for $\nu_1 = 0$ to react than for $\nu_1 = 1$, so that $\nu_1 = 0$ CHD_3 tends to slide further of the MEP than $\nu_1 = 1$ CHD_3. To observe this, see for

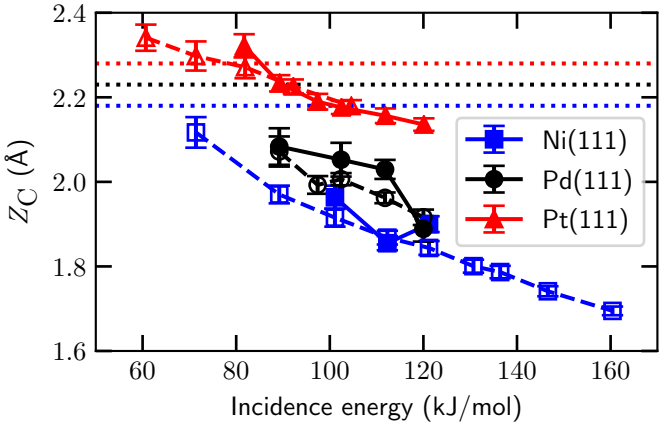

FIGURE 9.5: Distance of the carbon atom to the surface when a bond dissociates, i.e., when $r = r^{\ddagger}$, under laser-off conditions (solid lines) and for $\nu_1 = 1$ (dashed lines). The blue squares, black circles, and red triangles indicate Ni(111), Pd(111), and Pt(111), respectively. The horizontal dashed lines indicate the TS values. The error bars represent 68% confidence intervals.

example Figure 9.5 for Ni(111), observing the differences between laser-off conditions and $\nu_1 = 1$ for the lowest incidence energy for which a laser-off result is available on the one hand, and for the lowest incidence energy for which a $\nu_1 = 1$ result is available on the other hand, and Figure 9.2 to confirm that these conditions correspond to similar reaction probabilities. This has consequences for the vibrational efficacy, which is defined as the energy shift between the $\nu_1 = 1$ and $\nu_1 = 0$ (≈laser-off) reaction probability curves divided by the energy difference between $\nu_1 = 1$ and $\nu_1 = 0$, and defines how efficiently vibrational excitation promotes the reaction relative to increasing the translational energy. The larger bobsled effect on Ni(111) and Pd(111) than on Pt(111) partly explains why the vibrational efficacies for these systems (0.9 - 1.3 for Ni(111) and 0.7 - 0.9 for Pd(111)) exceed that obtained for Pt(111) (0.3 - 0.8, see Table 9.5, and also Ref. [12] for Ni(111) and Ref. [13] for Pt(111)). Furthermore, the large bobsled effect found for CHD_3 on Ni(111) is in line with one of the explanations Smith et al.[36] provided for the high vibrational efficacy of the asymmetric stretch mode of CH_4 reacting on Ni(111), i.e., that $\nu_3 = 1$ CH_4 reacts at the TS, while $\nu_3 = 0$ CH_4 slides off the MEP and has to pass over a higher barrier. Note that in the modeling of the reaction the molecule should be allowed to slide off the MEP to account for the bobsled effect on the vibrational efficacy. One reason that a too low

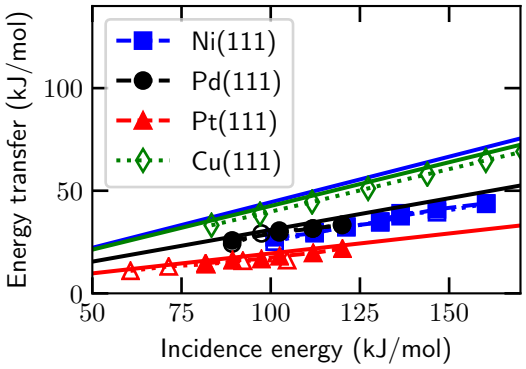

FIGURE 9.6: Energy transfer from methane to Ni(111) (blue squares), Pd(111) (black circles), Pt(111)[66] (red triangles), and Cu(111)[55] (green diamonds) compared to the refined Baule model. The solid lines without symbols indicate results predicted by the refined Baule model, whereas the dashed and dotted lines with solid and open symbols indicate laser-off and $\nu_1 = 1$ results, respectively.

vibrational efficacy was obtained for $\nu_3 = 1$ CH_4 on Ni(111) in Ref. [65] may have been that the RPH calculations used a harmonic approximation for motion orthogonal to the MEP and an expansion in harmonic vibrational eigenstates with up to one quantum only in all modes combined. It is possible that such a limited expansion is not capable of describing the effect that the molecule may slide off the reaction path, as perhaps indicated by the reaction probability of methane in its vibrational ground state becoming smaller for particular incidence energies if the expansion is enlarged to also contain states with up to two vibrational quanta[5].

As has also been suggested in Chapter 7, the MEP on Pd(111) is less favourable from a dynamical point of view than on Pt(111) due to the fact that the MEP makes a sharper turn on Pd(111) than on Pt(111). Therefore, it is expected that at low incidence energies and $\nu_1 = 1$ where dynamical effects such as the bobsled effect are less important, the reactivity on Pd(111) is similar to that on Pt(111), whereas at higher incidence energies and laser-off conditions dynamical effects cause the reactivity on Pd(111) to be similar to that on Ni(111) for the reaction of CHD_3 in its vibrational ground state (to which laser-off reaction bears a close resemblance at low nozzle temperature).

Another important dynamical aspect of the reaction of methane is the energy transfer from the molecule to the surface[55]. Figure 9.6 compares for scattered trajectories this energy transfer from CHD_3 to Cu(111)[55], Pt(111)[66], Ni(111)[12], and Pd(111). In general, it is observed that the lower the surface atom mass is, the higher the energy transfer is from methane to the surface atoms. This is also predicted by the hard sphere Baule model[67], where the mass ratio between the molecule and the surface atom plays a large role in the energy transfer. When the refined Baule model is employed, the following

average energy transfer (used in Figure 9.6) is obtained[68] (see Section 2.5).

$$\langle E_T \rangle = \frac{2.4\mu}{(1+\mu)^2} \langle E_i \rangle . \tag{9.2}$$

Here, $\mu = m/M$ (m is the mass of the projectile and M is the mass of a surface atom) and $\langle E_i \rangle$ is the average incidence energy. Surprisingly, the relatively simple Baule model does not only qualitatively but also semi-quantitatively predict the energy transfer from methane to the metal surfaces, except to Ni(111), in contrast to what was previously predicted[66]. Considering the close to spherical shape of methane, it is probable that the hard sphere approximation made by the Baule model will typically hold. This is also suggested by Figure 9.6, which shows remarkably good agreement of the computed energy transfer with that predicted by the refined Baule model for Pt, Pd, and Cu. Additional work will be required to test the validity of the refined Baule model for other systems and investigate the considerably lower energy transfer computed to Ni(111). Since the energy transfer from methane to Pd is higher than to Pt, less energy will be available for the reaction on Pd and thus the reaction probability should be further diminished on Pd compared to that on Pt. This effect will be larger at higher incidence energies as the difference in energy transfer between Pd and Pt will increase (see Figure 9.6). Moreover, as the computed energy transfer to Pd(111) and Ni(111) is predicted to be equal, differences in reaction probabilities on Pd(111) and Ni(111) are most likely not caused by the energy transfer from methane to the metal surface.

As can be seen from Figure 9.7, at high incidence energy the distribution of sites over which CHD_3 reacts on Pd(111) is close to statistical for both laser-off reaction and $\nu_1 = 1$. However, at lower incidence energy it is observed that the top site is the most reactive site, followed by the bridge site. This means that at lower incidence energy mostly only the minimum barrier is accessed, since it is located at the top site as discussed in Section 9.3.1. Therefore, at lower incidence energies a large portion of the surface would be catalytically inactive. This corresponds with the lack of increase in the reactivity of $\nu_1 = 1$ on Pd(111) from 102 to 112 kJ/mol, as it is also observed that the distribution of reaction sites shifts towards the less reactive sites (i.e., the bridge and hollow sites). Moreover, the reaction of CHD_3 on Pt(111) shows a similar site specific behaviour as CHD_3 reacting on Pd(111). At lower incidence energy the reaction on Ni(111) again occurs predominantly over the top site, however, the second most reactive site is now the hollow site instead of the bridge site. In general, all the considered metal surfaces show non-statistical behaviour, where the top site is usually favored, with the main difference

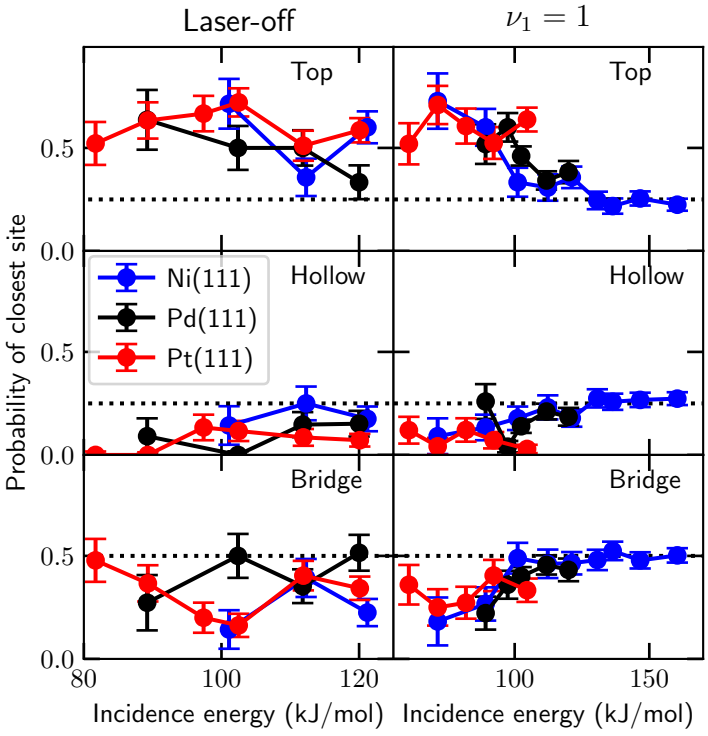

FIGURE 9.7: Fraction of closest high-symmetry site (i.e., top, hollow and bridge) to the impact site of reacting methane on Ni(111) (blue), Pd(111) (black), and Pt(111) (red) for laser-off and $\nu_1 = 1$ conditions, as a function of the incidence energy and when a bond dissociates, i.e., $r = r^{\ddagger}$. The dotted line indicates the statistical average for the high-symmetry site. The error bars represent 68% confidence intervals.

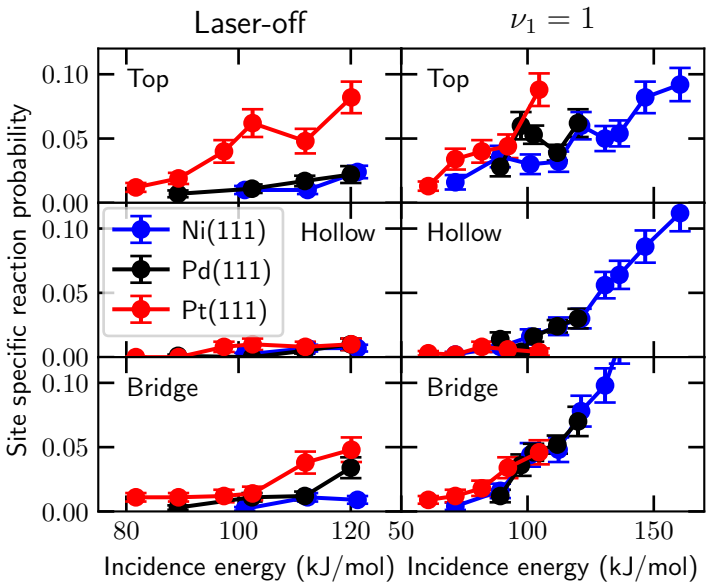

FIGURE 9.8: Reaction probability of CHD_3 on the high-symmetry sites (i.e., top, hollow and bridge) on Ni(111) (blue), Pd(111) (black), and Pt(111) (red) for laser-off conditions and for $\nu_1 = 1$ as a function of the incidence energy when a bond dissociates, i.e., $r = r^{\ddagger}$. The error bars represent 68% confidence intervals.

being the ordering of the sites according to their reactivity. This behaviour is also predicted by the site specific barriers discussed in Section 9.3.1.

Figure 9.8 shows site-specific reaction probabilities of CHD_3 which add up to total reaction probabilities. Again, Ni(111), Pd(111) and Pt(111) exhibit similar site-specific reaction probabilities. Most of the reactivity is observed above the top site, whereas the hollow and bridge sites play a considerably smaller role. Here the difference in reaction probability between Pd(111) and Pt(111) under laser-off conditions can be seen more clearly. The difference in reaction probability for the top site is large, whereas the difference for the hollow and bridge sites is generally much smaller. Therefore, the considerably lower reactivity of CHD_3 on Pd(111) than on Pt(111) under laser-off conditions is mostly due to the difference in the top site reactivity. However, this difference is not caused by the difference in minimum barrier heights; probably it is caused by the difference in barrier heights that can be dynamically accessed due to the bobsled effect. Furthermore, it remains unclear whether the large variation in reaction probability for Pd(111) and Ni(111) at the top site for $\nu_1 = 1$ is a statistical anomaly or a real physical feature. Also, the partial

TABLE 9.7: Dynamical features and how they qualitatively affect the reaction probability of CHD_3 on Ni(111), Pd(111), and Pt(111). The number of pluses and minuses indicate how much the effect increases or reduces the reaction probability, respectively, when the aforementioned surfaces are compared.

Dynamical feature	Ni(111)	Pd(111)	Pt(111)	Largest effect on
Bobsled effect	$---$	$---$	$-$	Laser-off
Energy transfer	$--$	$--$	$-$	Laser-off
Site specificity	$-$	$--$	$---$	Laser-off
Vibrational efficacy	$+++$	$++$	$+$	$\nu_1 = 1$
Angular distribution	$-$	$-$	$-$	Both

contribution of each site is compared to the total reaction probability for each surface in Figure 9.B.1, which again shows the aforementioned differences in site-specific reactivity.

While the difference between the low vibrational efficacy computed for CHD_3 + Pt(111) on the one hand and the higher vibrational efficacies on Pd(111) and Ni(111) on the other hand could be explained on the basis of the bobsled effect (see above), the reason for the higher vibrational efficacy on Ni(111) (0.9-1.3) than on Pd(111) (0.7-0.9, see Table 9.5) could not be explained in this way. On the basis of the minimum barrier heights and geometries collected in Table 9.2, it is tempting to speculate that the t2f site could play a role in this, as it has a much lower barrier on Ni(111) than on Pd(111), and a later barrier on Ni(111) than on Pd(111). The plot of the impact sites for the reactive trajectories with $\langle E_i \rangle = 89$ kJ/mol for $\nu_1 = 1$ on Ni(111) (Figure 9.B.2) can be construed to offer some support for this idea, as quite a few reactive impacts are seen near the corners of the triangles making up the t2f and t2h sites. However, to gather further support for this idea better statistics are needed, which can perhaps be obtained on the basis of QCT dynamics on a PES also incorporating the effect of surface atom motion, as has been done in Chapter 8 for CHD_3 + Cu(111).

In the reaction of CHD_3 on Pd(111), not much steering in the XY plane is observed (on average a movement of just 0.06 Å in the XY plane), as is typical for the reaction of CHD_3 on a metal surface[5, 12, 29, 52, 53]. As a result, it should be a good approximation to treat the reaction with a sudden approximation for motion in X and Y, as done for instance with the RPH model of Jackson and coworkers[5], and firmly established to be valid for CH_4 + Ni(111)[69], and also for H_2O + Ni(111)[70].

Finally, the general trends observed and how they affect the reaction probability are summarized in Table 9.7. First, the bobsled effect is considerably more important for Pd(111) and Ni(111) than for Pt(111), making Pt(111) considerably more reactive than the other surfaces, especially for laser-off conditions. Moreover, the energy transfer of methane to Pt(111) is smaller than to Pd(111) and Ni(111), again making Pt(111) relatively more reactive. However, the site-specific reactivity is increasingly more important when going from Ni(111) to Pt(111), reducing the reaction probability on Pt(111) the most. The vibrational efficacy plays an increasingly more important role when going from Pt(111) to Ni(111), increasing the reaction probability for $\nu_1 = 1$ on Ni(111) the most. Furthermore, the initial angular distribution of the molecule and concomitant steering are equally important on all surfaces considered here. These dynamical effects combined cause the reaction probability on Ni(111) and Pd(111) to be similar and on Pt(111) comparatively higher, for laser-off conditions. Additionally, they explain why the reactivity is rather similar on all of these surfaces for $\nu_1 = 1$. In this, it is suspected that the site-specificity plays the most important role in almost equalizing laser-off reaction on Pd(111) and Ni(111), while the vibrational efficacy should also be important to making the $\nu_1 = 1$ reaction probabilities almost equal on these two surfaces.

Due to the combined effects of decreased site-specificity and increased vibrational efficacy, it is conceivable that Ni(111) becomes more reactive than Pd(111), and/or Pd(111) becomes more reactive than Pt(111) towards $\nu_1 = 1$ CHD_3 at higher incidence energies than results are shown for in Figure 9.2b. It would be a considerable challenge to explore this experimentally, for two reasons[71, 72]: (i) At higher incidence energies, the extraction of the reactivity of $\nu_1 = 1$ CHD_3 requires a subtraction of an increasingly large "laser-off" signal from a "laser-on" signal that might actually decrease, because laser-excitation takes place from a rotational level that is less populated at the higher associated T_n, and (ii) the extraction requires the approximation that the reactivity of the vibrational ground state equals that averaged over the vibrational states populated in the beam under laser-off conditions, of which the validity decreases with incidence energy.

9.3.4 Discussion of Reactivity of Pd(111) vs Ni(111) and Pt(111); Comparison with Experiment

Experimentally, at low incidence energies ($< 70\,\mathrm{kJ/mol}$) (see Figure 9.9), the reactivity of Pd(111) towards CH_4 is similar to that of Pt(111), whereas Ni(111) is about three orders of magnitude less reactive than Pt(111)[23, 73–76]. It

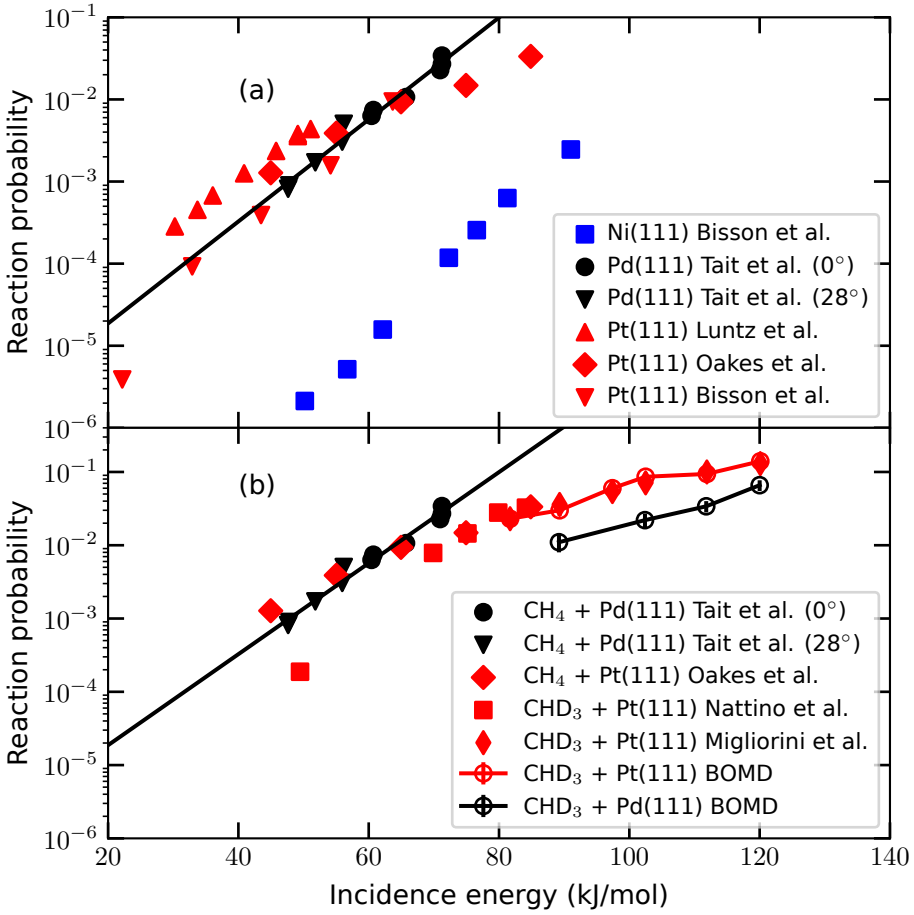

FIGURE 9.9: (a) Experimental reaction probability of CH_4 on Ni(111) (blue), Pd(111) (black) and Pt(111) (red) under laser-off conditions. Results for Ni(111) and Pt(111) are taken from Ref. [73] and Refs. [73–75], respectively. The Pd(111) results (black circles and triangles) are taken from Ref. [23], where the circles and triangles indicate an incidence angle of 0° and 28°, respectively, and the black line is a linear regression fit those points. (b) The reaction probability of CH_4 and CHD_3 on Pd(111) and Pt(111) obtained with experiment (closed symbols) and BOMD (open symbols) under laser-off conditions. For CH_4 + Pt(111) only the results from Ref. [75] are shown. The red squares and diamonds indicate results for CHD_3 + Pt(111) taken from Refs. [16] and [13], respectively.

TABLE 9.8: Seeding gas, surface temperature (T_s) and nozzle temperature (T_n) employed in the experiments shown Figure 9.9.

System	Author	Seeding gas	T_s (K)	T_n (K)
CH_4 + Ni(111)	Bisson et al.[73]	H_2	475	323 - 373
CH_4 + Pd(111)	Tait et al.[23]	He	550	470 - 885
CH_4 + Pt(111)	Luntz et al.[74]	H_2, He, Ar	800	300
CH_4 + Pt(111)	Oakes et al.[75]	He	550	500 - 1000
CH_4 + Pt(111)	Bisson et al.[73]	H_2	600	323 - 373
CHD_3 + Pt(111)	Nattino et al.[16]	He	120	500 - 850
CHD_3 + Pt(111)	Migliorini et al.[13]	H_2	500	400 - 650

should be noted that the experiments at low incidence energies were performed with CH_4 using various nozzle and surface temperatures (see Table 9.8), making a direct quantitative comparison between the experiments on CH_4 + Pt(111) and CH_4 + Pd(111), and with the BOMD results for CHD_3 difficult. Therefore, the general trends observed for the reaction of methane on Pt(111) are discussed here and we have tried to extrapolate this to Pd(111).

In Figure 9.9b a few results concerning Pt(111) and Pd(111) are shown in order to qualitatively compare the effect of nozzle and surface temperatures, and the isotopic effect of using CH_4 or CHD_3. Nattino et al.[16] used CHD_3 seeded in a He beam with $T_s = 120\,K$, whereas Migliorini et al.[13] used CHD_3 seeded in a H_2 beam with $T_s = 500\,K$. Typically, at the high incidence energies and reaction probabilities involved here, the surface temperature does not have a large effect on the reactivity of methane[55, 74, 77]. Moreover, at high surface temperature the seeding gas influences the kinetic energy and thus also the required nozzle temperature. Therefore, the slightly higher reaction probability of Nattino et al.[16] found for CHD_3 + Pt(111) in the overlapping regime is caused by the higher nozzle temperature (as needed by He-seeded molecular beam studies), as a larger fraction of CHD_3 in the beam will be vibrationally excited.

However, the surface temperature can cause the reaction probability at lower incidence energy to vary by up to two orders of magnitude, depending on the surface temperature and incidence energy[55, 65, 74, 77, 78]. This surface temperature effect probably causes the reaction probabilities obtained by Luntz and Bethune[74] ($T_s = 800\,K$) to be considerably higher than those obtained by Oakes et al.[75] ($T_s = 550\,K$) and Bisson et al.[73] ($T_s = 600\,K$), who all used CH_4. On the other hand, the higher reaction probability obtained by Oakes et al. ($T_n = 500 - 1000\,K$) compared to that by Bisson et al. ($T_n =$

323 − 373 K) is probably due to the higher employed nozzle temperature used by Oakes et al.

Furthermore, the effect of partially deuterating methane can be seen by comparing the results of Nattino et al. and Oakes et al. For the incidence energy range where data are available for both sets, the difference in surface temperature (i.e., $T_s = 120$ K and $T_s = 550$ K, respectively) should only play a role for the low incidence energies. Moreover, the nozzle temperature employed by Nattino et al. is similar to that by Oakes et al., and thus should not make a large difference either. It is expected that these differences should also (partially) cancel out at high incidence energies. It has also been shown previously that using CHD_3 instead of CH_4 lowers the reaction probability[74, 79–81]. However, the reaction probabilities obtained by Nattino et al. and Oakes et al. at high incidence energy are similar, where it is expected that the reaction probabilities obtained by Oakes et al. should be slightly higher than those by Nattino et al. It remains unclear why no difference at high incidence energy is observed between the two data sets, although it is possible that the molecular beams are considerably different making direct comparison difficult.

Finally, the reaction probability of CH_4 on Pd(111) obtained by Tait et al.[23] is similar to that of Oakes et al. for CH_4 + Pt(111), except for the highest incidence energies where Pd(111) is measured to be more reactive than Pt(111) towards methane. Both used the same surface temperature and similar nozzle temperature range, but Tait et al. used relatively less seeding gas and thus a higher nozzle temperature is employed for a given incidence energy compared to Oakes et al., which perhaps explains the higher reaction probability for Pd(111) at high incidence energy. At energies that are higher than those for which CH_4 + Pd(111) experimental results are available, the BOMD calculations in this chapter predict a substantially lower reactivity of Pd(111) towards CHD_3 than that of Pt(111). While this may seem odd in light of the experimental results for CH_4 on Pt(111) and Pd(111), one should keep in mind that due to the simulated use of H_2 seeding the incidence energy is higher while the nozzle temperature is lower for the calculations on CHD_3 + Pd(111) and Pt(111), which leads to a larger importance of the bobsled effect and to a smaller importance of the promotion of reaction by vibrational excitation. Both effects disfavor the reaction on Pd(111). Nevertheless, experiments are clearly needed to verify the predictions for the reaction of CHD_3 on Pd(111). For all of these reasons it is concluded that experimentally it is expected that the reactivity of CHD_3 + Pd(111) should be slightly lower than that of CHD_3 + Pt(111) at lower incidence energies. Qualitatively, this is also what is obtained from the BOMD calculations at higher incidence energies, although there the

difference in reactivity is larger (see Figure 9.2).

9.4 Conclusions

In this chapter, predictive calculations using BOMD have been performed for CHD_3 on Pd(111) with the SRP32-vdW functional. The reactivity of Pd(111) is compared to that of Pt(111) and Ni(111), and is found to be intermediate between these systems. Although this is to be expected from the minimum barrier heights and experiments at low incidence energy, the reaction probability is also found to be dependent on dynamical effects such as the bobsled effect and energy transfer from methane to the metal surface. In general, at the lowest incidence energy and laser-off conditions when these dynamical effects are smaller, the reaction probability on Pd(111) is comparable to that on Pt(111), which is also observed by experiment. However, at higher incidence energies, these dynamical effects play a larger role and the reaction probability on Pd(111) is more comparable to that on Ni(111). Furthermore, for $\nu_1 = 1$ all three systems investigated show similar reaction probabilities. Moreover, barriers across the surface need to be considered as the reaction of methane on a group 10 metal surface is highly site specific, with the minimum barrier height and geometry varying across the surface. This variation in barrier heights across the surface also explains the similarity of the reactivity of Ni(111) and Pd(111) towards methane at high incidence energy. Interestingly, methane on Pd(111) and Ni(111) exhibits typically quite similar dynamical behaviour such as the bobsled effect, energy transfer from methane to the surface, and the site-specific reactivity, whereas the dynamical behaviour of methane on Pt(111) tends to be different from that on the aforementioned metal surfaces. This again causes reactivity of Pd(111) towards methane to shift more to that of Ni(111) than that of Pt(111). These results also suggest why Pt-Cu(111) is predicted to be much more reactive than Pd-Cu(111) at high incidence energy in Chapter 7. Hopefully, these predictions will inspire new experiments that will test the transferability of the SRP32-vdW functional to CHD_3 + Pd(111).

Appendix

9.A Convergence

Figure 9.A.1 and Table 9.A.1 show the convergence of the minimum barrier height for methane dissociation on Pd(111) (E_b) as a function of the number of layers for different numbers of k-points using a kinetic energy cut-off of 400 eV, yielding a converged barrier height of 82.8 kJ/mol. The computational set up employed in the BOMD calculations (4 layers, 3×3 surface unit cell, $6 \times 6 \times 1$ k-points, kinetic energy cut-off of 400 eV, 13 Å vacuum distance) yields a barrier height of 84.1 kJ/mol. It is confirmed that the computational set up is also converged with respect to the kinetic energy cut-off.

9.B Site-Specific Reaction Probability

Figure 9.B.1 shows the same site-specific reaction probabilities of CHD_3 for each investigated surface as in Figure 9.8, but here every surface is shown separately under laser-off and $\nu_1 = 1$ conditions, showing how the site-specific reaction probabilities add up to the total reaction probability. Moreover, the impact site of the reacting methane on Ni(111), Pd(111) and Pt(111) is shown in Figure 9.B.2 for a reaction probability of about 2.5% and 5.0% under laser-off and $\nu_1 = 1$ conditions, respectively. Note that for laser-off conditions 1000 trajectories were run and for $\nu_1 = 1$ 500 trajectories were run. Here it can be seen that under laser-off conditions, most of the reaction occurs near the top site, even if the reaction occurs in the hollow or bridge region, whereas for $\nu_1 = 1$ conditions the reaction occurs across most of the surface.

TABLE 9.A.1: Convergence of the minimum barrier height (kJ/mol) on Pd(111) is shown as a function of the amount of layers, *k*-points, and the size of the surface unit cell (3×3 and 4×4) for a plane wave energy cutoff of 400 eV. The results obtained with the employed computational set up in the BOMD is in bold and the most converged result (i.e., obtained with the largest setup) is in italic.

Layers	*k*-points	$E_{b,3\times3}$	$E_{b,4\times4}$
4	$3 \times 3 \times 1$		80.6
4	$4 \times 4 \times 1$	81.1	86.8
4	$6 \times 6 \times 1$	**84.1**	84.5
4	$8 \times 8 \times 1$	85.1	85.6
4	$10 \times 10 \times 1$	85.4	
5	$3 \times 3 \times 1$		80.2
5	$4 \times 4 \times 1$	80.8	86.1
5	$6 \times 6 \times 1$	85.3	85.1
5	$8 \times 8 \times 1$	85.1	84.9
5	$10 \times 10 \times 1$	85.3	
6	$3 \times 3 \times 1$		83.1
6	$4 \times 4 \times 1$	82.5	82.6
6	$6 \times 6 \times 1$	83.4	83.5
6	$8 \times 8 \times 1$	83.6	83.5
6	$10 \times 10 \times 1$	83.8	
7	$3 \times 3 \times 1$		79.4
7	$4 \times 4 \times 1$	81.4	84.7
7	$6 \times 6 \times 1$	83.6	83.4
7	$8 \times 8 \times 1$	84.2	83.7
7	$10 \times 10 \times 1$	84.7	
8	$3 \times 3 \times 1$		81.2
8	$4 \times 4 \times 1$	81.7	84.2
8	$6 \times 6 \times 1$	84.2	83.5
8	$8 \times 8 \times 1$	83.9	83.4
8	$10 \times 10 \times 1$	84.2	
9	$3 \times 3 \times 1$		81.1
9	$4 \times 4 \times 1$	82.5	83.2
9	$6 \times 6 \times 1$	82.9	82.9
9	$8 \times 8 \times 1$	84.0	83.5
9	$10 \times 10 \times 1$	84.3	
10	$3 \times 3 \times 1$		80.1
10	$4 \times 4 \times 1$	81.1	85.1
10	$6 \times 6 \times 1$	82.8	83.0
10	$8 \times 8 \times 1$	83.7	*82.8*
10	$10 \times 10 \times 1$	84.1	

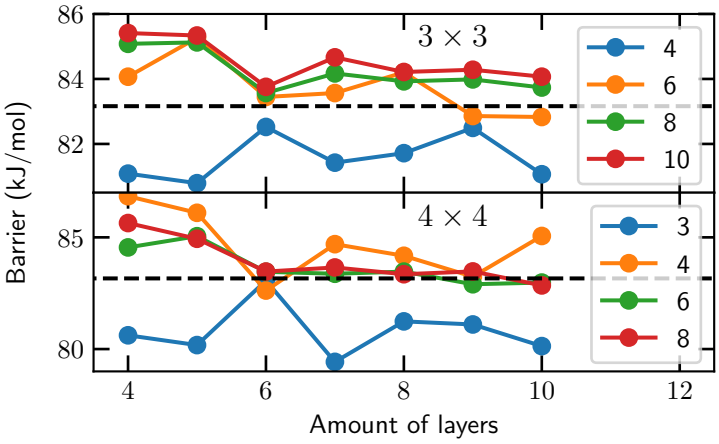

FIGURE 9.A.1: Convergence of the minimum barrier height on Pd(111) as a function of the amount of layers for the number of k-points equal to $(n \times n \times 1)$, where n is indicated in the legend. The upper panel and lower panel used a 3×3 and 4×4 supercell, respectively. The dashed lines indicate the converged barrier height.

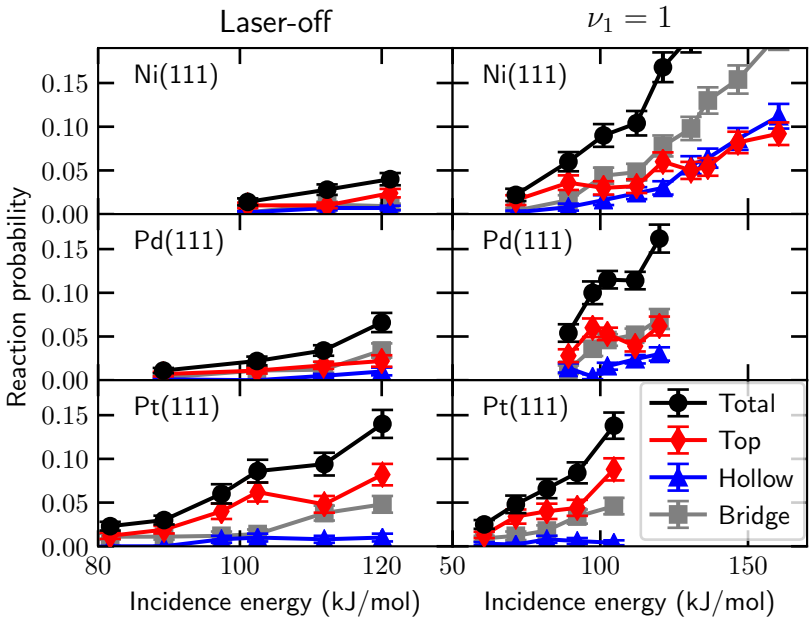

FIGURE 9.B.1: Reaction probability of CHD_3 on the top, hollow and bridge high-symmetry sites (red, blue and grey, respectively) and the total reaction probability (black) on Ni(111), Pd(111) and Pt(111) for laser-off conditions and for $\nu_1 = 1$, as a function of the incidence energy when a bond dissociates, i.e., $r = r^{\ddagger}$. The error bars represent 68% confidence intervals.

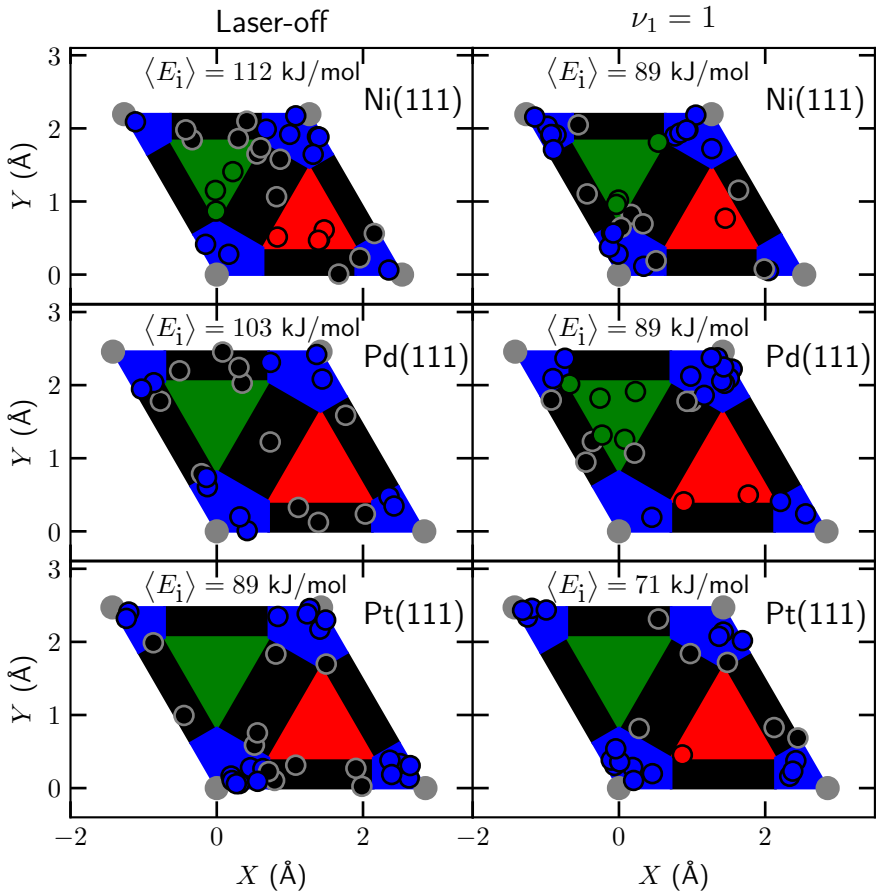

FIGURE 9.B.2: Impact site of reacting CHD_3 on Ni(111), Pd(111) and Pt(111) for laser-off and $\nu_1 = 1$ when a bond dissociates, i.e., $r = r^{\ddagger}$. Under laser-off conditions the reaction probability is about 2.5%, whereas for the $\nu_1 = 1$ conditions the reaction probability is about 5%. The top, fcc, hcp and bridge sites are indicated in blue, red, green and black, respectively, and the top layer atoms are indicate by the gray circles.

References

(1) Rostrup-Nielsen, J. R.; Sehested, J.; Nørskov, J. K. In *Advances in Catalysis*; Academic Press: 2002; Vol. 47, pp 65–139, DOI: 10.1016/S0360-0564(02)47006-X.

(2) Wei, J.; Iglesia, E. Mechanism and Site Requirements for Activation and Chemical Conversion of Methane on Supported Pt Clusters and Turnover Rate Comparisons among Noble Metals. *J. Phys. Chem. B* **2004**, *108*, 4094–4103, DOI: 10.1021/jp036985z.

(3) Jones, G.; Jakobsen, J. G.; Shim, S. S.; Kleis, J.; Andersson, M. P.; Rossmeisl, J.; Abild-Pedersen, F.; Bligaard, T.; Helveg, S.; Hinnemann, B.; Rostrup-Nielsen, J. R.; Chorkendorff, I.; Sehested, J.; Nørskov, J. K. First Principles Calculations and Experimental Insight into Methane Steam Reforming over Transition Metal Catalysts. *J. Catal.* **2008**, *259*, 147–160, DOI: 10.1016/j.jcat.2008.08.003.

(4) Kroes, G.-J. Towards Chemically Accurate Simulation of Molecule–Surface Reactions. *Phys. Chem. Chem. Phys.* **2012**, *14*, 14966–14981, DOI: 10.1039/C2CP42471A.

(5) Jackson, B.; Nattino, F.; Kroes, G.-J. Dissociative Chemisorption of Methane on Metal Surfaces: Tests of Dynamical Assumptions Using Quantum Models and Ab Initio Molecular Dynamics. *J. Chem. Phys.* **2014**, *141*, 054102, DOI: 10.1063/1.4891327.

(6) Wellendorff, J.; Silbaugh, T. L.; Garcia-Pintos, D.; Nørskov, J. K.; Bligaard, T.; Studt, F.; Campbell, C. T. A Benchmark Database for Adsorption Bond Energies to Transition Metal Surfaces and Comparison to Selected DFT Functionals. *Surf. Sci.* **2015**, *640*, 36–44, DOI: 10.1016/j.susc.2015.03.023.

(7) Gautier, S.; Steinmann, S. N.; Michel, C.; Fleurat-Lessard, P.; Sautet, P. Molecular Adsorption at Pt(111). How Accurate Are DFT Functionals? *Phys. Chem. Chem. Phys.* **2015**, *17*, 28921–28930, DOI: 10.1039/C5CP04534G.

(8) Kroes, G.-J. Toward a Database of Chemically Accurate Barrier Heights for Reactions of Molecules with Metal Surfaces. *J. Phys. Chem. Lett.* **2015**, *6*, 4106–4114, DOI: 10.1021/acs.jpclett.5b01344.

(9) Díaz, C.; Pijper, E.; Olsen, R. A.; Busnengo, H. F.; Auerbach, D. J.; Kroes, G. J. Chemically Accurate Simulation of a Prototypical Surface Reaction: H_2 Dissociation on Cu(111). *Science* **2009**, *326*, 832–834, DOI: 10.1126/science.1178722.

(10) Sementa, L.; Wijzenbroek, M.; van Kolck, B. J.; Somers, M. F.; Al-Halabi, A.; Busnengo, H. F.; Olsen, R. A.; Kroes, G. J.; Rutkowski, M.; Thewes, C.; Kleimeier, N. F.; Zacharias, H. Reactive Scattering of H_2 from Cu(100): Comparison of Dynamics Calculations Based on the Specific Reaction Parameter Approach to Density Functional Theory with Experiment. *J. Chem. Phys.* **2013**, *138*, 044708, DOI: 10.1063/1.4776224.

(11) Ghassemi, E. N.; Wijzenbroek, M.; Somers, M. F.; Kroes, G.-J. Chemically Accurate Simulation of Dissociative Chemisorption of D_2 on Pt(111). *Chem. Phys. Lett.* **2017**, *683*, 329–335, DOI: 10.1016/j.cplett.2016.12.059.

(12) Nattino, F.; Migliorini, D.; Kroes, G.-J.; Dombrowski, E.; High, E. A.; Killelea, D. R.; Utz, A. L. Chemically Accurate Simulation of a Polyatomic Molecule-Metal Surface Reaction. *J. Phys. Chem. Lett.* **2016**, *7*, 2402–2406, DOI: 10.1021/acs.jpclett.6b01022.

(13) Migliorini, D.; Chadwick, H.; Nattino, F.; Gutiérrez-González, A.; Dombrowski, E.; High, E. A.; Guo, H.; Utz, A. L.; Jackson, B.; Beck, R. D.; Kroes, G.-J. Surface Reaction Barriometry: Methane Dissociation on Flat and Stepped Transition-Metal Surfaces. *J. Phys. Chem. Lett.* **2017**, *8*, 4177–4182, DOI: 10.1021/acs.jpclett.7b01905.

(14) Chadwick, H.; Gutiérrez-González, A.; Migliorini, D.; Beck, R. D.; Kroes, G.-J. Incident Angle Dependence of CHD_3 Dissociation on the Stepped Pt(211) Surface. *J. Phys. Chem. C* **2018**, *122*, 19652–19660, DOI: 10.1021/acs.jpcc.8b05887.

(15) Chadwick, H.; Guo, H.; Gutiérrez-González, A.; Menzel, J. P.; Jackson, B.; Beck, R. D. Methane Dissociation on the Steps and Terraces of Pt(211) Resolved by Quantum State and Impact Site. *J. Chem. Phys.* **2018**, *148*, 014701, DOI: 10.1063/1.5008567.

(16) Nattino, F.; Ueta, H.; Chadwick, H.; van Reijzen, M. E.; Beck, R. D.; Jackson, B.; van Hemert, M. C.; Kroes, G.-J. Ab Initio Molecular Dynamics Calculations versus Quantum-State-Resolved Experiments on CHD_3 + Pt(111): New Insights into a Prototypical Gas–Surface Reaction. *J. Phys. Chem. Lett.* **2014**, *5*, 1294–1299, DOI: 10.1021/jz500233n.

(17) Nave, S.; Jackson, B. Vibrational Mode-Selective Chemistry: Methane Dissociation on Ni(100). *Phys. Rev. B* **2010**, *81*, 233408, DOI: 10.1103/PhysRevB.81.233408.

(18) Nattino, F.; Migliorini, D.; Bonfanti, M.; Kroes, G.-J. Methane Dissociation on Pt(111): Searching for a Specific Reaction Parameter Density Functional. *J. Chem. Phys.* **2016**, *144*, 044702, DOI: 10.1063/1.4939520.

(19) Czakó, G.; Bowman, J. M. Dynamics of the Reaction of Methane with Chlorine Atom on an Accurate Potential Energy Surface. *Science* **2011**, *334*, 343–346, DOI: 10.1126/science.1208514.

(20) Goodman, R. M.; Farrell, H. H.; Somorjai, G. A. Mean Displacement of Surface Atoms in Palladium and Lead Single Crystals. *J. Chem. Phys.* **1968**, *48*, 1046–1051, DOI: 10.1063/1.1668759.

(21) Manson, J. R. Inelastic Scattering from Surfaces. *Phys. Rev. B* **1991**, *43*, 6924–6937, DOI: 10.1103/PhysRevB.43.6924.

(22) Manson, J. R. Multiphonon Atom-Surface Scattering. *Comput. Phys. Commun.* **1994**, *80*, 145–167, DOI: 10.1016/0010-4655(94)90101-5.

(23) Tait, S. L.; Dohnálek, Z.; Campbell, C. T.; Kay, B. D. Methane Adsorption and Dissociation and Oxygen Adsorption and Reaction with CO on Pd Nanoparticles on MgO(100) and on Pd(111). *Surf. Sci.* **2005**, *591*, 90–107, DOI: 10.1016/j.susc.2005.06.024.

(24) Groß, A. Reactivity of Bimetallic Systems Studied from First Principles. *Top. Catal.* **2006**, *37*, 29–39, DOI: 10.1007/s11244-006-0005-x.

(25) Ramos, M.; Martínez, A. E.; Busnengo, H. F. H_2 Dissociation on Individual Pd Atoms Deposited on Cu(111). *Phys. Chem. Chem. Phys.* **2012**, *14*, 303–310, DOI: 10.1039/C1CP22163A.

(26) Marcinkowski, M. D.; Darby, M. T.; Liu, J.; Wimble, J. M.; Lucci, F. R.; Lee, S.; Michaelides, A.; Flytzani-Stephanopoulos, M.; Stamatakis, M.; Sykes, E. C. H. Pt/Cu Single-Atom Alloys as Coke-Resistant Catalysts for Efficient C–H Activation. *Nat. Chem.* **2018**, *10*, 325–332, DOI: 10.1038/nchem.2915.

(27) Marcus, R. A. On the Analytical Mechanics of Chemical Reactions. Quantum Mechanics of Linear Collisions. *J. Chem. Phys.* **1966**, *45*, 4493–4499, DOI: 10.1063/1.1727528.

(28) McCullough, E. A.; Wyatt, R. E. Quantum Dynamics of the Collinear (H, H_2) Reaction. *J. Chem. Phys.* **1969**, *51*, 1253–1254, DOI: 10.1063/1.1672133.

(29) Gerrits, N.; Migliorini, D.; Kroes, G.-J. Dissociation of CHD_3 on Cu(111), Cu(211), and Single Atom Alloys of Cu(111). *J. Chem. Phys.* **2018**, *149*, 224701, DOI: 10.1063/1.5053990.

(30) Killelea, D. R.; Campbell, V. L.; Shuman, N. S.; Utz, A. L. Bond-Selective Control of a Heterogeneously Catalyzed Reaction. *Science* **2008**, *319*, 790–793, DOI: 10.1126/science.1152819.

(31) Shen, X. J.; Lozano, A.; Dong, W.; Busnengo, H. F.; Yan, X. H. Towards Bond Selective Chemistry from First Principles: Methane on Metal Surfaces. *Phys. Rev. Lett.* **2014**, *112*, 046101, DOI: 10.1103/PhysRevLett.112.046101.

(32) Hundt, P. M.; Ueta, H.; van Reijzen, M. E.; Jiang, B.; Guo, H.; Beck, R. D. Bond-Selective and Mode-Specific Dissociation of CH_3D and CH_2D_2 on Pt(111). *J. Phys. Chem. A* **2015**, *119*, 12442–12448, DOI: 10.1021/acs.jpca.5b07949.

(33) Gutiérrez-González, A.; Crim, F. F.; Beck, R. D. Bond Selective Dissociation of Methane (CH_3D) on the Steps and Terraces of Pt(211). *J. Chem. Phys.* **2018**, *149*, 074701, DOI: 10.1063/1.5041349.

(34) Beck, R. D.; Maroni, P.; Papageorgopoulos, D. C.; Dang, T. T.; Schmid, M. P.; Rizzo, T. R. Vibrational Mode-Specific Reaction of Methane on a Nickel Surface. *Science* **2003**, *302*, 98–100, DOI: 10.1126/science.1088996.

(35) Juurlink, L. B. F.; Killelea, D. R.; Utz, A. L. State-Resolved Probes of Methane Dissociation Dynamics. *Prog. Surf. Sci.* **2009**, *84*, 69–134, DOI: 10.1016/j.progsurf.2009.01.001.

(36) Smith, R. R.; Killelea, D. R.; DelSesto, D. F.; Utz, A. L. Preference for Vibrational over Translational Energy in a Gas-Surface Reaction. *Science* **2004**, *304*, 992–995, DOI: 10.1126/science.1096309.

(37) Jiang, B.; Yang, M.; Xie, D.; Guo, H. Quantum Dynamics of Polyatomic Dissociative Chemisorption on Transition Metal Surfaces: Mode Specificity and Bond Selectivity. *Chem. Soc. Rev.* **2016**, *45*, 3621–3640, DOI: 10.1039/C5CS00360A.

(38) Yoder, B. L.; Bisson, R.; Beck, R. D. Steric Effects in the Chemisorption of Vibrationally Excited Methane on Ni(100). *Science* **2010**, *329*, 553–556, DOI: 10.1126/science.1191751.

(39) Gutiérrez-González, A.; Torio, M. E.; Busnengo, H. F.; Beck, R. D. Site Selective Detection of Methane Dissociation on Stepped Pt Surfaces. *Top. Catal.* **2019**, DOI: 10.1007/s11244-019-01170-5.

(40) Kresse, G.; Hafner, J. Ab Initio Molecular-Dynamics Simulation of the Liquid-Metal–Amorphous-Semiconductor Transition in Germanium. *Phys. Rev. B* **1994**, *49*, 14251–14269, DOI: 10.1103/PhysRevB.49.14251.

(41) Kresse, G.; Hafner, J. Ab Initio Molecular Dynamics for Liquid Metals. *Phys. Rev. B* **1993**, *47*, 558–561, DOI: 10.1103/PhysRevB.47.558.

(42) Kresse, G.; Furthmüller, J. Efficient Iterative Schemes for Ab Initio Total-Energy Calculations Using a Plane-Wave Basis Set. *Phys. Rev. B* **1996**, *54*, 11169–11186, DOI: 10.1103/PhysRevB.54.11169.

(43) Kresse, G.; Furthmüller, J. Efficiency of Ab-Initio Total Energy Calculations for Metals and Semiconductors Using a Plane-Wave Basis Set. *Comput. Mater. Sci.* **1996**, *6*, 15–50, DOI: 10.1016/0927-0256(96)00008-0.

(44) Kresse, G.; Joubert, D. From Ultrasoft Pseudopotentials to the Projector Augmented-Wave Method. *Phys. Rev. B* **1999**, *59*, 1758–1775, DOI: 10.1103/PhysRevB.59.1758.

(45) Blöchl, P. E. Projector Augmented-Wave Method. *Phys. Rev. B* **1994**, *50*, 17953–17979, DOI: 10.1103/PhysRevB.50.17953.

(46) Methfessel, M.; Paxton, A. T. High-Precision Sampling for Brillouin-Zone Integration in Metals. *Phys. Rev. B* **1989**, *40*, 3616–3621, DOI: 10.1103/PhysRevB.40.3616.

(47) Henkelman, G.; Jónsson, H. A Dimer Method for Finding Saddle Points on High Dimensional Potential Surfaces Using Only First Derivatives. *J. Chem. Phys.* **1999**, *111*, 7010–7022, DOI: 10.1063/1.480097.

(48) Heyden, A.; Bell, A. T.; Keil, F. J. Efficient Methods for Finding Transition States in Chemical Reactions: Comparison of Improved Dimer Method and Partitioned Rational Function Optimization Method. *J. Chem. Phys.* **2005**, *123*, 224101, DOI: 10.1063/1.2104507.

(49) Kästner, J.; Sherwood, P. Superlinearly Converging Dimer Method for Transition State Search. *J. Chem. Phys.* **2008**, *128*, 014106, DOI: 10.1063/1.2815812.

(50) Xiao, P.; Sheppard, D.; Rogal, J.; Henkelman, G. Solid-State Dimer Method for Calculating Solid-Solid Phase Transitions. *J. Chem. Phys.* **2014**, *140*, 174104, DOI: 10.1063/1.4873437.

(51) Transition State Tools Package for VASP https://theory.cm.utexas.edu/vtsttools/index.html (accessed 02/08/2021).

(52) Migliorini, D.; Chadwick, H.; Kroes, G.-J. Methane on a Stepped Surface: Dynamical Insights on the Dissociation of CHD_3 on Pt(111) and Pt(211). *J. Chem. Phys.* **2018**, *149*, 094701, DOI: 10.1063/1.5046065.

(53) Chadwick, H.; Gutiérrez-González, A.; Beck, R. D.; Kroes, G.-J. Transferability of the SRP32-vdW Specific Reaction Parameter Functional to CHD_3 Dissociation on Pt(110)-(2x1). *J. Chem. Phys.* **2019**, *150*, 124702, DOI: 10.1063/1.5081005.

(54) Chadwick, H.; Gutiérrez-González, A.; Beck, R. D.; Kroes, G.-J. CHD_3 Dissociation on the Kinked Pt(210) Surface: A Comparison of Experiment and Theory. *J. Phys. Chem. C* **2019**, *123*, 14530–14539, DOI: 10.1021/acs.jpcc.9b03051.

(55) Gerrits, N.; Shakouri, K.; Behler, J.; Kroes, G.-J. Accurate Probabilities for Highly Activated Reaction of Polyatomic Molecules on Surfaces Using a High-Dimensional Neural Network Potential: CHD_3 + Cu(111). *J. Phys. Chem. Lett.* **2019**, *10*, 1763–1768, DOI: 10.1021/acs.jpclett.9b00560.

(56) Perdew, J. P.; Burke, K.; Ernzerhof, M. Generalized Gradient Approximation Made Simple. *Phys. Rev. Lett.* **1996**, *77*, 3865–3868, DOI: 10.1103/PhysRevLett.77.3865.

(57) Hammer, B.; Hansen, L. B.; Nørskov, J. K. Improved Adsorption Energetics within Density-Functional Theory Using Revised Perdew-Burke-Ernzerhof Functionals. *Phys. Rev. B* **1999**, *59*, 7413–7421, DOI: 10.1103/PhysRevB.59.7413.

(58) Dion, M.; Rydberg, H.; Schröder, E.; Langreth, D. C.; Lundqvist, B. I. Van Der Waals Density Functional for General Geometries. *Phys. Rev. Lett.* **2004**, *92*, 246401, DOI: 10.1103/PhysRevLett.92.246401.

(59) Mondal, A.; Wijzenbroek, M.; Bonfanti, M.; Díaz, C.; Kroes, G.-J. Thermal Lattice Expansion Effect on Reactive Scattering of H_2 from Cu(111) at T_s = 925 K. *J. Phys. Chem. A* **2013**, *117*, 8770–8781, DOI: 10.1021/jp4042183.

(60) Touloukian, Y.; Kirby, R.; Taylor, R.; Desai, P., Thermophysical Properties of Matter - the TPRC Data Series. Volume 12. Thermal Expansion Metallic Elements and Alloys, 14 vols.; Plenum Publishing Corporation: New York, 1975; Vol. 12; 1436 pp.

(61) Nave, S.; Tiwari, A. K.; Jackson, B. Methane Dissociation and Adsorption on Ni(111), Pt(111), Ni(100), Pt(100), and Pt(110)-(1x2): Energetic Study. *J. Chem. Phys.* **2010**, *132*, 054705, DOI: 10.1063/1.3297885.

(62) Nave, S.; Jackson, B. Methane Dissociation on Ni(111) and Pt(111): Energetic and Dynamical Studies. *J. Chem. Phys.* **2009**, *130*, 054701, DOI: 10.1063/1.3065800.

(63) Fisher, R. A. On the Interpretation of X^2 from Contingency Tables, and the Calculation of P. *J. R. Stat. Soc.* **1922**, *85*, 87–94, DOI: 10.2307/2340521.

(64) Jackson, B.; Nave, S. The Dissociative Chemisorption of Methane on Ni(100): Reaction Path Description of Mode-Selective Chemistry. *J. Chem. Phys.* **2011**, *135*, 114701, DOI: 10.1063/1.3634073.

(65) Guo, H.; Jackson, B. Mode-Selective Chemistry on Metal Surfaces: The Dissociative Chemisorption of CH_4 on Pt(111). *J. Chem. Phys.* **2016**, *144*, 184709, DOI: 10.1063/1.4948941.

(66) Chadwick, H.; Migliorini, D.; Kroes, G. J. CHD_3 Dissociation on Pt(111): A Comparison of the Reaction Dynamics Based on the PBE Functional and on a Specific Reaction Parameter Functional. *J. Chem. Phys.* **2018**, *149*, 044701, DOI: 10.1063/1.5039458.

(67) Baule, B. Theoretische Behandlung Der Erscheinungen in Verdünnten Gasen. *Ann. Phys.* **1914**, *349*, 145–176, DOI: 10.1002/andp.19143490908.

(68) Goodman, F. O.; Wachman, H. Y. *Formula for Thermal Accommodation Coefficient*; 66-1; Cambridge, Massachusetts: M.I.T. Fluid Dynamics Research, 1966, DOI: 10.21236/ad0631007.

(69) Shen, X.; Zhang, Z.; Zhang, D. H. Communication: Methane Dissociation on Ni(111) Surface: Importance of Azimuth and Surface Impact Site. *J. Chem. Phys.* **2016**, *144*, 101101, DOI: 10.1063/1.4943128.

(70) Jiang, B.; Guo, H. Dynamics of Water Dissociative Chemisorption on Ni(111): Effects of Impact Sites and Incident Angles. *Phys. Rev. Lett.* **2015**, *114*, 166101, DOI: 10.1103/PhysRevLett.114.166101.

(71) Juurlink, L. B. F.; McCabe, P. R.; Smith, R. R.; DiCologero, C. L.; Utz, A. L. Eigenstate-Resolved Studies of Gas-Surface Reactivity: CH_4 ν_3 Dissociation on Ni(100). *Phys. Rev. Lett.* **1999**, *83*, 868–871, DOI: 10.1103/PhysRevLett.83.868.

(72) Schmid, M. P.; Maroni, P.; Beck, R. D.; Rizzo, T. R. Surface Reactivity of Highly Vibrationally Excited Molecules Prepared by Pulsed Laser Excitation: CH_4 ($2\nu_3$) on Ni(100). *J. Chem. Phys.* **2002**, *117*, 8603–8606, DOI: 10.1063/1.1519860.

(73) Bisson, R.; Sacchi, M.; Dang, T. T.; Yoder, B.; Maroni, P.; Beck, R. D. State-Resolved Reactivity of $CH_4(2\nu_3)$ on Pt(111) and Ni(111): Effects of Barrier Height and Transition State Location. *J. Phys. Chem. A* **2007**, *111*, 12679–12683, DOI: 10.1021/jp076082w.

(74) Luntz, A. C.; Bethune, D. S. Activation of Methane Dissociation on a Pt(111) Surface. *J. Chem. Phys.* **1989**, *90*, 1274–1280, DOI: 10.1063/1.456132.

(75) Oakes, D. J.; McCoustra, M. R.; Chesters, M. A. Dissociative Adsorption of Methane on Pt(111) Induced by Hyperthermal Collisions. *Faraday Discuss.* **1993**, *96*, 325–336, DOI: 10.1039/FD9939600325.

(76) Higgins, J.; Conjusteau, A.; Scoles, G.; Bernasek, S. L. State Selective Vibrational ($2\nu 3$) Activation of the Chemisorption of Methane on Pt (111). *J. Chem. Phys.* **2001**, *114*, 5277–5283, DOI: 10.1063/1.1349895.

(77) Campbell, V. L.; Chen, N.; Guo, H.; Jackson, B.; Utz, A. L. Substrate Vibrations as Promoters of Chemical Reactivity on Metal Surfaces. *J. Phys. Chem. A* **2015**, *119*, 12434–12441, DOI: 10.1021/acs.jpca.5b07873.

(78) Tiwari, A. K.; Nave, S.; Jackson, B. The Temperature Dependence of Methane Dissociation on Ni(111) and Pt(111): Mixed Quantum-Classical Studies of the Lattice Response. *J. Chem. Phys.* **2010**, *132*, 134702, DOI: 10.1063/1.3357415.

(79) Beebe, T. P.; Goodman, D. W.; Kay, B. D.; Yates, J. T. Kinetics of the Activated Dissociative Adsorption of Methane on the Low Index Planes of Nickel Single Crystal Surfaces. *J. Chem. Phys.* **1987**, *87*, 2305–2315, DOI: 10.1063/1.453162.

(80) Lee, M. B.; Yang, Q. Y.; Ceyer, S. T. Dynamics of the Activated Dissociative Chemisorption of CH_4 and Implication for the Pressure Gap in Catalysis: A Molecular Beam–High Resolution Electron Energy Loss Study. *J. Chem. Phys.* **1987**, *87*, 2724–2741, DOI: 10.1063/1.453060.

(81) Holmblad, P. M.; Wambach, J.; Chorkendorff, I. Molecular Beam Study of Dissociative Sticking of Methane on Ni(100). *J. Chem. Phys.* **1995**, *102*, 8255–8263, DOI: 10.1063/1.468955.